

## Supplementary Information

### **Intrinsic Defects at Interface of FAPbI<sub>3</sub>/MAPbI<sub>3</sub> Superlattice: Insight from First-Principles Calculation**

Liping Cheng<sup>a,b</sup>, Baoen Xu<sup>c</sup>, Yanli Zeng<sup>a\*</sup>, Lingpeng Meng<sup>a\*</sup>

*<sup>a</sup>Hebei Key Laboratory of Inorganic Nano-materials, College of Chemistry and Materials  
Science, Hebei Normal University, Shijiazhuang 050024, PR China*

*<sup>b</sup>College of Chemistry and Chemical Engineering, Xingtai University, Xingtai, 054001,  
PR China*

*<sup>c</sup>Technology Innovation Center of Hebei Province for Heterocyclic Compound, College of  
Chemical Engineering, Shijiazhuang University, Shijiazhuang 050035, PR China*

## Computational methods for properties

The effective masses of the holes and electrons at VBM and CBM, and the reduced effective masses were calculated by Eqs. S1 and 2<sup>1</sup>

$$m^* = \hbar^2 \left( \frac{\partial^2 \varepsilon(k)}{\partial k^2} \right)^{-1} \quad \text{S(1)}$$

$$m_r^* = \frac{m_e^* m_h^*}{m_e^* + m_h^*} \quad \text{S(2)}$$

where  $\varepsilon(k)$  is the band energy of VBM or CBM, and  $k$  is the inverse lattice vector. Wannier exciton model was adopted to calculate the exciton binding energy<sup>2</sup>

$$E_{eb} = \frac{m_r^* e^4}{2\hbar^2 \varepsilon_\infty^2} = 13.6 \frac{m_r^*}{\varepsilon_\infty^2} \quad \text{S(3)}$$

where  $m_r^*$  is the reduced effective mass, and  $\varepsilon_\infty$  is static dielectric constant at zero frequency approximation and it can be calculated by following equation<sup>3</sup>

$$\varepsilon_\infty(\hat{q}, \omega) \approx \lim_{q \rightarrow 0} \varepsilon_{0,0}(\mathbf{q}, \omega) \quad \text{S(4)}$$

where  $\omega$  is the optical frequency and  $q$  is the electron momentum operator.

The linear optical properties<sup>4</sup> of semiconductors can be calculated using the frequency-dependent complex dielectric function  $\varepsilon(\omega)$

$$\varepsilon(\omega) = \varepsilon_1(\omega) + i\varepsilon_2(\omega) \quad \text{S(5)}$$

where  $\omega$  is the optical frequency,  $\varepsilon_1$  and  $\varepsilon_2$  are the real and imaginary parts of the dielectric function, respectively. In the one-electron graph, the imaginary part of the dielectric function  $\varepsilon_2(\omega)$  can be obtained from the following equation:

$$\varepsilon_2(\omega) = \frac{4\pi^2 e^2}{\Omega} \lim_{q \rightarrow 0} \frac{1}{q^2} \sum_{c,v,k} 2w_k \delta(E_c - E_v - \omega) |\langle c | \mathbf{e} \cdot \mathbf{q} | v \rangle|^2 \quad \text{S(6)}$$

where  $\langle c | \mathbf{e} \cdot \mathbf{q} | v \rangle$  is the integral optical transition from the valence state ( $v$ ) to the conduction state ( $c$ ),  $e$  denotes the polarization direction of the photon and  $q$  is the electron momentum operator. The integral on  $k$  is the sum of special  $k$  points with weighting factor  $w_k$ . The real part of the dielectric function  $\varepsilon_1(\omega)$  can be gained from the Kramers-Kronig relation<sup>4</sup>

$$\varepsilon_1(\omega) = 1 + \frac{2}{\pi} P \int_0^\infty \frac{\varepsilon_2(\omega') \omega'}{\omega'^2 - \omega^2 + i\eta} d\omega' \quad \text{S(7)}$$

where  $P$  is the principle value and  $\eta$  is the complex shift parameter. The absorption

coefficients can be computed by the following equation<sup>5</sup>:

$$\alpha(\omega) = \sqrt{2\omega} \sqrt{\sqrt{\varepsilon_1^2(\omega) + \varepsilon_2^2(\omega)} - \varepsilon_1(\omega)} \quad \text{S(8)}$$

Open-circuit voltage  $V_{OC}$ , short-circuit current  $J_{SC}$ , and theoretical power conversion efficiency PCE ( $\eta$ ) were calculated by Eqs. S9-12. The maximum short-circuit current  $J_{SC}$  is calculated on the assumption that all incident photons with energy greater than the superlattice band gap are absorbed,<sup>6</sup>

$$J_{SC} = e \int_{E_g}^{\infty} \frac{S(E)}{E} dE \quad \text{S(9)}$$

where  $e$ ,  $E$ , and  $S(E)$  are the electronic charge, the energy of an incident photon, and the incident spectral power per unit area, respectively. The open circuit voltage  $V_{OC}$  can be estimated by

$$V_{OC} = (E_g - E_{loss}) / e \quad \text{S(10)}$$

in which  $E_{loss}$  is the loss-in-potential and 0.5 eV is adopted similar to the previous report.<sup>7</sup> The maximum theoretical PCE ( $\eta$ ) can be obtained by  $J$ ,  $V_{OC}$ , fill factor ( $FF$ ), and the total incident power density ( $P_{sun}$ ).<sup>8</sup>

$$\eta(E_g) = \frac{FF \times J_{SC} \times V_{OC}}{P_{sun}} \quad \text{S(11)}$$

$$P_{sun} = \int_0^{\infty} S(E) dE \quad \text{S(12)}$$

According to the solar spectrum data meter provided by the National Renewable Energy Laboratory<sup>9</sup>, the  $P_{sun}$  is taken as 100 mW/cm<sup>2</sup>. The fill factor  $FF$  is taken as the reported experimental value of 0.731.<sup>9</sup>

Table S1. Calculated band gaps (eV) of MAPbI<sub>3</sub> and FAPbI<sub>3</sub> using PBE, PBE+SOC and HSE06+SOC compared with experimental values (in brackets).

	PBE	PBE+SOC	HSE06+SOC
MAPbI <sub>3</sub>	1.687 (1.61) <sup>11</sup>	0.666	1.575
FAPbI <sub>3</sub>	1.418 (1.43) <sup>12</sup>	0.342	1.320

Table S2. Calculated lattice parameters and average monolayer thickness in perovskites and superlattice.

perovskites	<i>a b c</i> (Å)	$\alpha \beta \gamma$ (degree)	$d_{\text{MAPbI}_3}$ (Å)	$d_{\text{FAPbI}_3}$ (Å)
MAPbI <sub>3</sub>	6.340, 6.330, 6.388 (6.311, 6.311, 6.316) <sup>13</sup>	90.0, 90.8, 89.9	6.340	
FAPbI <sub>3</sub>	6.489, 6.311, 6.396 (6.42 <sup>13</sup> , 6.36 <sup>15</sup> )	90.0, 90.0, 90.0		6.489
(FAPbI <sub>3</sub> ) <sub>2</sub> /(MAPbI <sub>3</sub> ) <sub>2</sub>	25.596, 6.319, 6.388	89.9, 90.1, 90.1	6.447	6.352

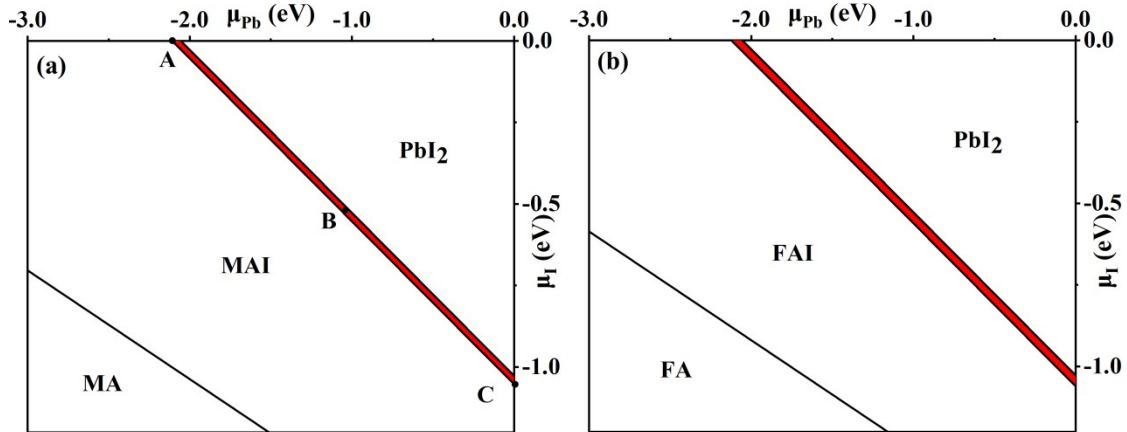
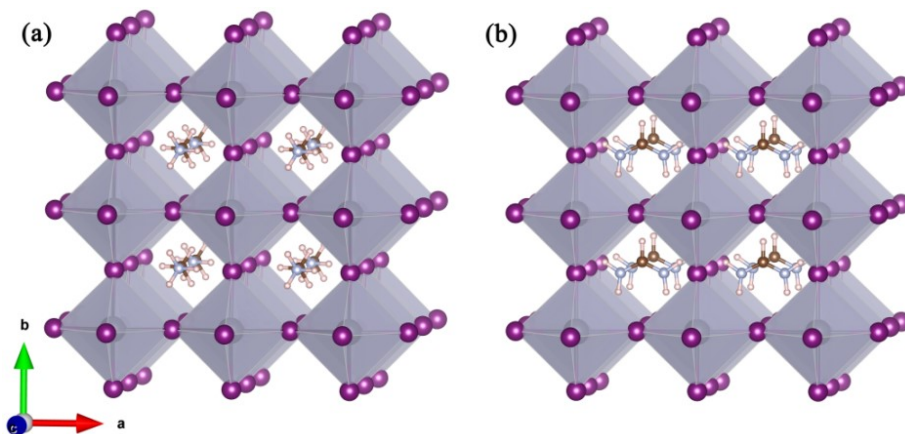
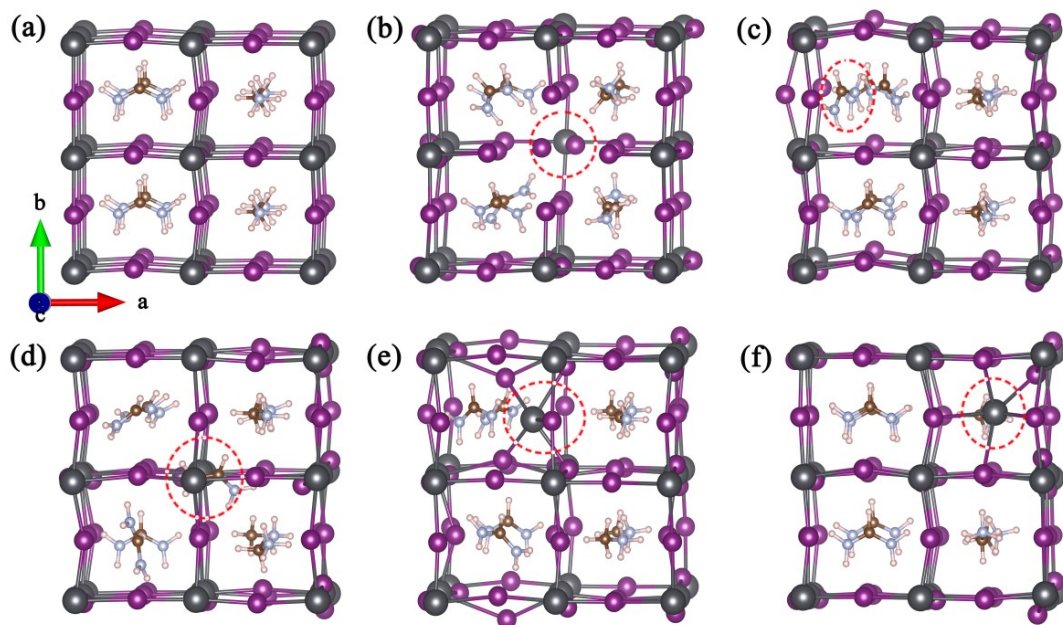


Fig. S1. Chemical potential region for the thermal equilibrium growth of (a) MAPbI<sub>3</sub> and (b) FAPbI<sub>3</sub> crystal.



**Fig. S2.** The bulk models of  $2 \times 2 \times 2$  supercell used to calculate electrostatic potentials for MAPbI<sub>3</sub> and FAPbI<sub>3</sub>.



**Fig. S3.** Local structures of FAPbI<sub>3</sub>/MAPbI<sub>3</sub> superlattice with (a) defect free, (b) V<sub>Pb</sub><sup>2-</sup>, (c) FA<sub>i</sub><sup>+</sup>, (d) FA<sub>I</sub><sup>2+</sup>, (e) Pb<sub>I</sub><sup>3+</sup>, (f) Pb<sub>MA</sub><sup>+</sup>.

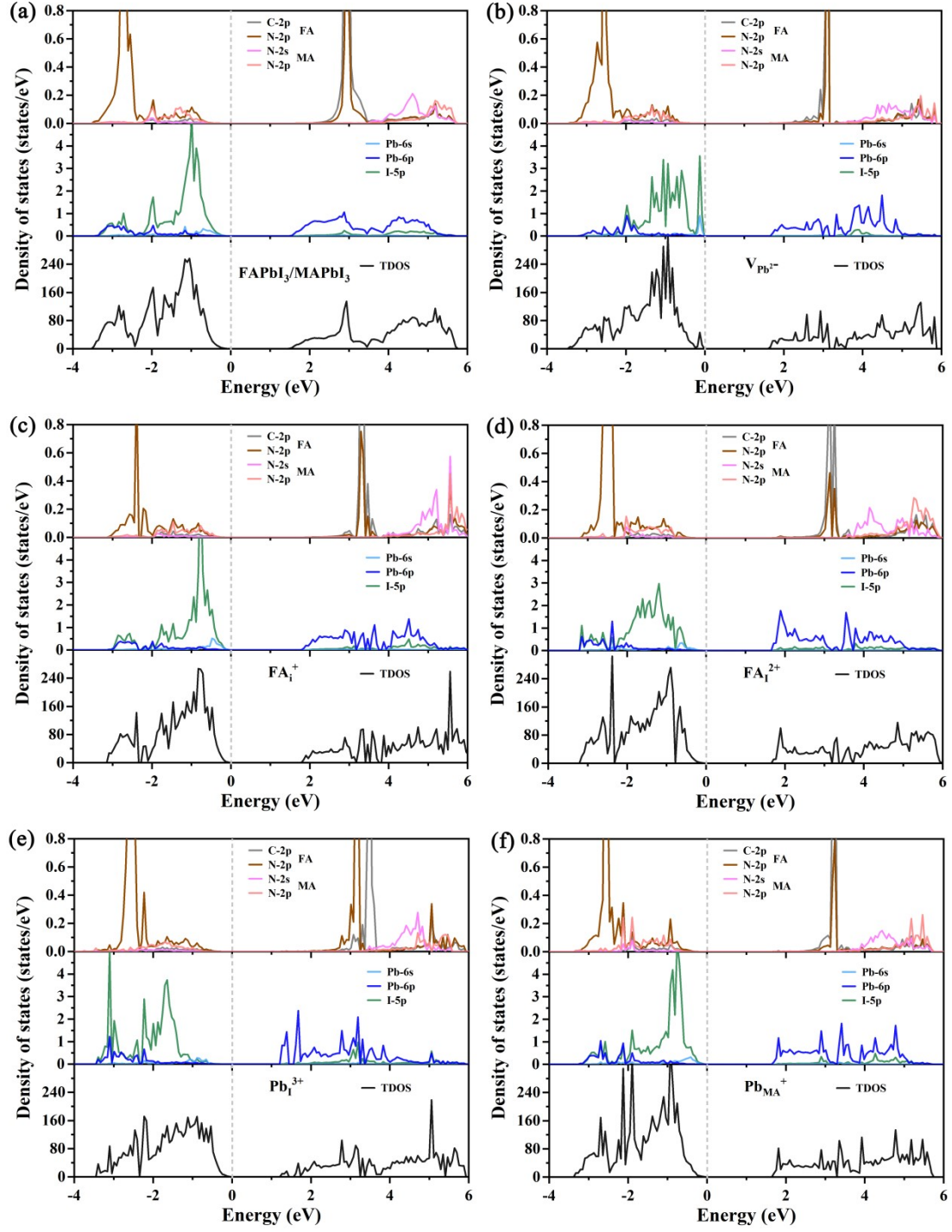


**Fig. S4.** TDOS and PDOS of superlattice with (a) defect free, (b)  $V_{\text{Pb}^{2-}}$ , (c)  $\text{FA}_i^+$ , (d)  $\text{FA}_I^{2+}$ , (e)  $\text{Pb}_I^{3+}$ , (f)  $\text{Pb}_{\text{MA}}^+$ . The Fermi level is set to zero (the gray dotted line).

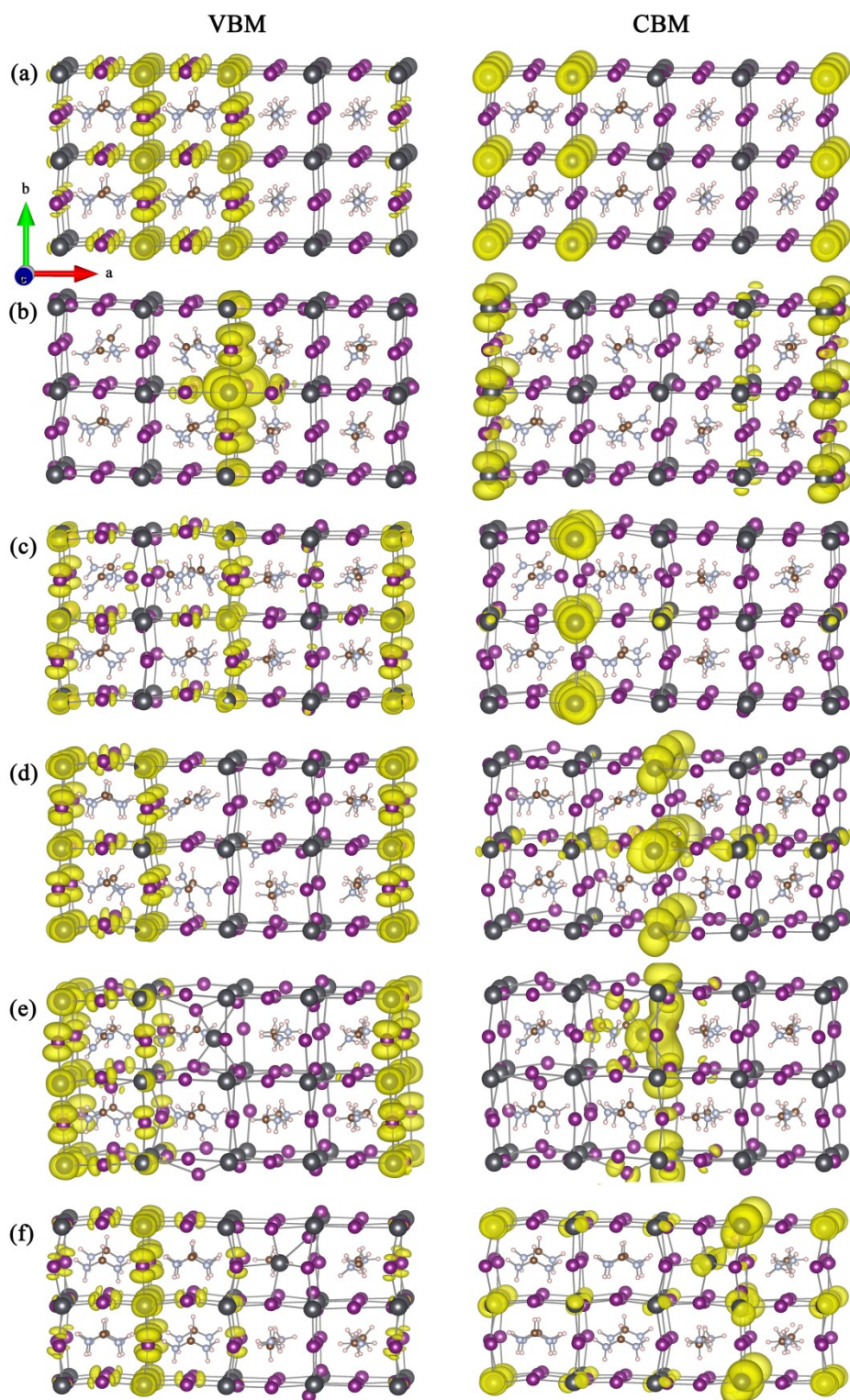


**Fig. S5.** Band decomposed charge densities distributions of VBM (with an isosurface value of  $0.0001 \text{ e}\text{\AA}^{-3}$ ) and CBM (with an isosurface value of  $0.0002 \text{ e}\text{\AA}^{-3}$ ) for the superlattices with and without defects. (a) perfect, (b)  $\text{V}_{\text{pb}}^{2-}$ , (c)  $\text{FA}_{\text{I}}^{+}$ , (d)  $\text{FA}_{\text{I}}^{2+}$ , (e)  $\text{Pb}_{\text{I}}^{3+}$ , (f)  $\text{Pb}_{\text{MA}}^{+}$ .

## References:

- 1 Y. Zhao, X. Wang, B. Liu, Z. Yu, P. He, Q. Wan, M. Cai and H. Yu, Geometric structure and photovoltaic properties of mixed halide germanium perovskites from theoretical view, *Org. Electron.*, 2018, **53**, 50-56.
- 2 J. Even, L. Pedesseau and C. Katan, Analysis of Multivalley and Multibandgap Absorption and Enhancement of Free Carriers Related to Exciton Screening in Hybrid Perovskites, *J. Phys. Chem. C*, 2014, **118**, 11566-11572.
- 3 M. Gajdoš, K. Hummer, G. Kresse, J. Furthmüller and F. Bechstedt, Linear optical properties in the projector-augmented wave methodology, *Physical review. B*, 2006, **73**, 45112.
- 4 V. Wang, N. Xu, J. Liu, G. Tang and W. Geng, VASPKIT: A user-friendly interface facilitating high-throughput computing and analysis using VASP code, *Comput. Phys. Commun.*, 2021, **267**, 108033.
- 5 S. H. Wemple and M. DiDomenico, Behavior of the Electronic Dielectric Constant in Covalent and Ionic Materials, *Phys. Rev. B*, 1971, **3**, 1338-1351.
- 6 H. J. Snaith, Estimating the Maximum Attainable Efficiency in Dye-Sensitized Solar Cells, *Adv. Funct. Mater.*, 2010, **20**, 13-19.
- 7 X. Ma and Z. Li, The effect of oxygen molecule adsorption on lead iodide perovskite surface by first-principles calculation, *Appl. Surf. Sci.*, 2018, **428**, 140-147.
- 8 W. Shockley and H. J. Queisser, Detailed Balance Limit of Efficiency of p-n Junction Solar Cells, *J. Appl. Phys.*, 1961, **32**, 510-519.
- 9 Source: Data from United States Department of Energy, National Renewable Energy Laboratory, Reference Solar Spectral Irradiance: Air Mass 1.5. <http://rredc.nrel.gov/solar/spectra/am1.5> (accessed: July 2021).
- 10 J. Han, S. Luo, X. Yin, Y. Zhou, H. Nan, J. Li, X. Li, D. Oron, H. Shen and H. Lin, Hybrid PbS Quantum-Dot-in-Perovskite for High-Efficiency Perovskite Solar Cell, *Small*, 2018, **14**, 1801016.
- 11 Y. Yamada, T. Nakamura, M. Endo, A. Wakamiya and Y. Kanemitsu, Near-band-edge optical responses of solution-processed organic-inorganic hybrid perovskite  $\text{CH}_3\text{NH}_3\text{PbI}_3$  on

- mesoporous TiO<sub>2</sub> electrodes, *Appl. Phys. Express*, 2014, **7**.
- 12 S. Pang, H. Hu, J. Zhang, S. Lv, Y. Yu, F. Wei, T. Qin, H. Xu, Z. Liu and G. Cui, NH<sub>2</sub>CH=NH<sub>2</sub>PbI<sub>3</sub>: An Alternative Organolead Iodide Perovskite Sensitizer for Mesoscopic Solar Cells, *Chem. Mater.*, 2014, **26**, 1485-1491.
- 13 C. C. Stoumpos, C. D. Malliakas and M. G. Kanatzidis, Semiconducting Tin and Lead Iodide Perovskites with Organic Cations: Phase Transitions, High Mobilities, and Near-Infrared Photoluminescent Properties, *Inorg. Chem.*, 2013, **52**, 9019-9038.
- 14 Y. Guo, C. Li, X. Li, Y. Niu, S. Hou and F. Wang, Effects of Rb Incorporation and Water Degradation on the Stability of the Cubic Formamidinium Lead Iodide Perovskite Surface: A First-Principles Study, *J. Phys. Chem. C*, 2017, **121**, 12711-12717.
- 15 M. T. Weller, O. J. Weber, J. M. Frost and A. Walsh, Cubic Perovskite Structure of Black Formamidinium Lead Iodide,  $\alpha$ -[HC(NH<sub>2</sub>)<sub>2</sub>]PbI<sub>3</sub>, at 298 K, *J. Phys. Chem. Lett.*, 2015, **6**, 3209-3212.